Article

Not peer-reviewed version

Experimental Study of White Light Interferometry in Mach-Zehnder Interferometers Based on Standard Single Mode Fiber

J. L. Cano-Perez *, J. Gutierrez-Gutiérrez *, C. Perezcampos-Mayoral, E. Perez-Campos, M. S. Pina-Canseco, L. Tepech-Carrillo, M. Vargas-Treviño, E. I. Guerra-Hernandez, A. Martinez-Helmes, J. M. Estudillo-Ayala, J. M. Sierra-Hernandez, R. Rojas-Laguna

Posted Date: 14 March 2024

doi: 10.20944/preprints202403.0858.v1

Keywords: White light interference, bi-tapers and core-offset Mach-Zehnder interferometer.

Article

Experimental Study of White Light Interferometry in Mach-Zehnder Interferometers Based on Standard Single Mode Fiber

J. L. Cano-Perez [1,*], J. Gutiérrez-Gutiérrez [2,*], C. Perezcampos-Mayoral [1], E. Pérez-Campos [3], M. S. Pina-Canseco [4], L. Tepech-Carrillo [2], M. Vargas-Treviño [2], E. I. Guerra-Hernández [2], A. Martínez-Helmes [5], J. M. Estudillo-Ayala [6], J. M. Hernandez-Sierra [6] and R. Rojas-Laguna [6]

[1] Doctorado en Biociencias, Facultad de Medicina y Cirugia; Universidad Autónoma "Benito Juárez" de Oaxaca. Ex Hacienda de Aguilera S/N, Calz. San Felipe del Agua, Oaxaca de Juárez, C.P. 68120, Mexico; cpecmay@uabjo.mx (C.P.-M.)

[2] Facultad de Sistemas Biologicos e Innovacion Tecnologica, Universidad Autónoma "Benito Juárez" de Oaxaca (FASBIT-UABJO), Av. Universidad S/N, Ex-Hacienda 5 Señores, Oaxaca de Juárez, C.P. 68120, Mexico; ltepech@uabjo.mx (L.T.-C.); mvargas.cat@uabjo.mx (M.V.-T.); ghernandez.cat@uabjo.mx (E.I.G.-H.)

[3] National Technology of Mexico / IT. Oaxaca Mexico. perezcampos@prodigy.net.mx; pcampos@itoaxaca.edu.mx (E.P.-C.)

[4] Facultad de Medicina y Cirugia, Universidad Autónoma "Benito Juárez" de Oaxaca. Ex Hacienda de Aguilera S/N, Calz. San Felipe del Agua, Oaxaca de Juárez, C.P. 68120, Mexico; perezcampos123@yahoo.es (E.P.-C.); mpina.cat@uabjo.mx (S.P.-C.).

[5] Facultad de Contaduría y Administración, Universidad Autónoma "Benito Juárez" de Oaxaca (FCA-UABJO), Av. Universidad S/N, Ex-Hacienda 5 Señores, Oaxaca de Juárez, C.P. 68120, Mexico. amartinez@uabjo.mx (A.M.-H.)

[6] Division de Ingenierias, campus Irapuato-Salamanca, Universidad de Guanajuato, Carretera Salamanca-Valle de Santiago km 3.5 + 1.8, Comunidad de Palo Blanco, Salamanca, Gto., C.P. 36885, Mexico; jm.sierrahernandez@ugto.mx (J.M.S.-H.); julian@ugto.mx (J.M.E.-A.); rlaguna@ugto.mx (R.L.-R)

* Correspondence: jcano@uabjo.mx (J.L.C.-P.); jgutierrez.cat@uabjo.mx (J.G.-G)

Abstract: The technique of optical interferometry has many applications in various fields of knowledge, including astronomy, optical metrology, biology, and chemistry. The visible interference pattern of a conventional single mode fiber (SMF-28) tapered and core-offset structured in-line Mach-Zehnder interferometer has been demonstrated. The white source is generated by an LED, with a wavelength range of 400 nm to 650 nm emission. We analyze the performance of the interference emission with a waist length of 1.8 mm to 6 mm and with a waist diameter of 10 μm to 60 μm for the tapered structure. The achieved visibility is V=0.14 with an FSR of 23 nm. The core-offset structure interferometer is analyzed with different displacements in x and y axis and with a separation length L of 2.5 cm, 4.0 cm and 5.0 cm between two core joints. The output interference emission has a visibility of V= 0.3, V=0.27 and V=0.34 with an FSR of 23 nm, 17 nm and 8 nm, respectively. The sensitivity obtained from the temperature sensor is of 3.53 a.u./°C, with R^2 of 0.99769. The proposed MZIs are low cost and can be used for implementation of sensing system in the field as the industry and medical applications.

Keywords: white light interference; bi-tapers and core-offset Mach-Zehnder interferometer

1. Introduction

The technique of optical interferometry, is widely used in the fabrication of fiber optic sensors due to its accurate measurement of physical quantities of industrial and medical fields. Optical interferometry, is based on the interference of two or more beams from a light source launched into dielectric media with different optical length paths. As a result, an optical phase difference is created between the beams, and the interference pattern is obtained [1]. A very small change in the optical path difference induces a change in the interference light intensity to the output sensor, one can get

 doi:10.20944/preprints202403.0858.v1

the information of about these changes for the measurement of physical parameters. The optical fiber sensor based on in-line Mach-Zehnder interferometer (MZI) have become more attractive research, this due to its simplicity, adaptability, manufacturing, compact size and stability. They are usually fabricated using single mode fiber (SMF) [2-7], multimode fiber (MMF) [8-13], photonic crystal fiber [14-16], erbium doped fiber (EDF) [7,17] and with different configurations, core offset [2-4], tapers [5-7,17] , two peanut-shape [7,18], microcavities [19-21] and other structures. In general, the MZIs are used to measure several physical variables, such as curvature [2,17], refractive index [3,5-7], temperature [4,18], strain [14] and gas sensing [16]. The optical fiber MZIs have been studied main in the far-infrared (FIR) [1-9,14-18], near-infrared (NIR) [19,20], and the visible spectrum (VIS). There has been little research on the design of interferometric sensors based on optical fiber [19-21]. The NIR and VIS interference has been researched by Eftimov et al., [19,20], and they used optical fiber SM800 and SM600, the spectrum interference is obtained in the range of 670 nm to 1100 nm. The interference emission in the VIS region is obtained in taper MZI based in microfiber or nanofiber (MNFs), and the MZI is fabricated with two MNFs that are placed on a MgF_2 substrate [21]. The supercontinuum source is used in their experimental setup [19-21].

In this work, in-line MZIs were proposed and experimentally demonstrated an emission pattern of interference with white light from an LED source. For visible light interference research, two MZIs with a structure SMF-SMF-SMF were fabricated, the first interferometer was constructed bi-taper and another interferometer based on core-offset splicing technique, both MZIs was fabricated by standard optical fiber (SMF-28) and is analyzed their interference emission individually.

2. Design and Fabrication of Mach-Zehnder Interferometer

Two interferometers were proposed and fabricated to white light analysis interference, taper and core-offset in-line MZI.

2.1. Design and Fabrication of Taper MZI

The tapered MZI was fabricated using a home stretching machine that s simultaneously heats and stretches a short section of single mode fiber (SMF-28 of Thorlabs, with 8.2 μm, 125 μm of core and cladding diameters, respectively and an operating wavelength range of 1260 nm to 1650 nm). The flames are generated with a precise mixture of butane and oxygen gas. The section of SMF is fixed at both ends by two holders, these holders are on a servomotor. A computer controls a machine stretching, here the main parameter is introduced by means of a home software (the main parameter introduced to the taper is only one: the waist diameter), Figure 1.

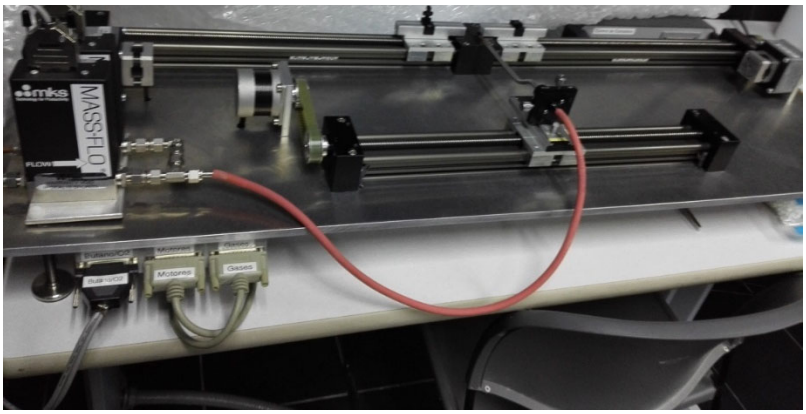

Figure 1. Home machine stretching to fabricate the tapers (Designed and build at Laboratory of fiber optics, Universitat de València).

With this, we can create a region of fiber with small and uniform waist, where the fiber diameter changes as a result of the stretching to create an adiabatic tapered MZI [5].

 doi:10.20944/preprints202403.0858.v1

Figure 2 shows the schematic of a bi-taper MZI, which consists of a single-mode fiber and can be divided into first taper T_1 and second taper T_2, with a separation distance L. The tapers T_1 and T_2, can be divided into regions: down taper (D_{down1} and D_{down2}), waist length (L_1 and L_2), waist diameter (W_1 and W_2) and up-taper (D_{up1} and D_{down2}), respectively; $D_1 = D_{down1} = D_{up1}$ and $D_2 = D_{down2} = D_{up2}$. The tapers T_1 and T_2, can be divided into regions: down and up-taper ($D_{1,2}$), waist length ($L_{1,2}$), waist diameter ($W_{1,2}$), respectively. In an SMF, coherent light propagates along the core and the fundamental mode (LP_{01}) is generated, but when a low-coherence source is launched into the SMF, higher-order modes (LP_{0m}) are excited [10,11]. The interference effects may exist between different core modes or between different cladding modes of the MZI structure. The modal interference between modes of the MZI structure can be given by [11-13]:

$$I = I_1 + I_2 + 2\sqrt{I_1 * I_2}\cos(\theta) \quad (1)$$

where I_1 and I_2 are the intensities of the interference signal, the core modes and the cladding modes, respectively. θ is the phase difference between the core mode and the cladding mode, and is given by:

$$\theta = \frac{2\pi\,(\Delta n_{eff})\,L}{\lambda} \quad (2)$$

where λ is the wavelength of the light source, L is the fiber waist length of the MZI, and the $\Delta n_{eff} = n_{eff}^{core} - n_{eff}^{clad}$ is the refractive index difference of the two interferometer arms, where n_{eff}^{core} and n_{eff}^{clad} are the effective refractive index of the core and cladding modes of the fiber, respectively When the interference signal reaches its minimum at $\theta = \pi(2m + 1)$ in the equation (1), the wavelength of the mth order attenuation peak is written as in the equation (2). As a result, the free spectral range (FSR) of such a fiber interferometer is expressed as [7,15]:

$$FSR = \frac{\lambda^2}{\Delta n_{eff}} L \quad (3)$$

Several MZIs with a different length L and waist diameter were fabricated and their transmission spectra were analyzed.

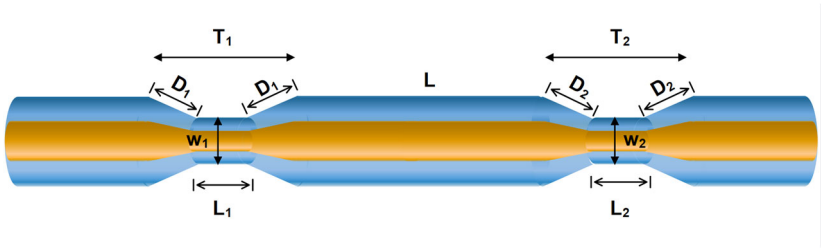

Figure 2. Schematic bi-taper MZI on SMF-28.

The experimental setup for analyzing the pattern interference in the VIS region of MZIs is shown in the Figure 3, an LED source (DLF, Model LP3WBCD, power of 3 Watts, natural white) with a wavelength range of 400 nm to 650 nm (the spectral emission is shown in Figure 4). The light is introduced into fiber optics with an Olympus Plan N 20x/0.40 micro-scope objective, which is mounted on fiber alignment 3-axis flexure stages (MBT610/N), them, the light travels through in MZI and the spectral emission interference is obtained by Spectrum Analyzer (Ocean Optics, USB650) with a slit of 5 in the software configuration of the computer.

Preprints.org (www.preprints.org) | NOT PEER-REVIEWED | Posted: 14 March 2024 doi:10.20944/preprints202403.0858.v1

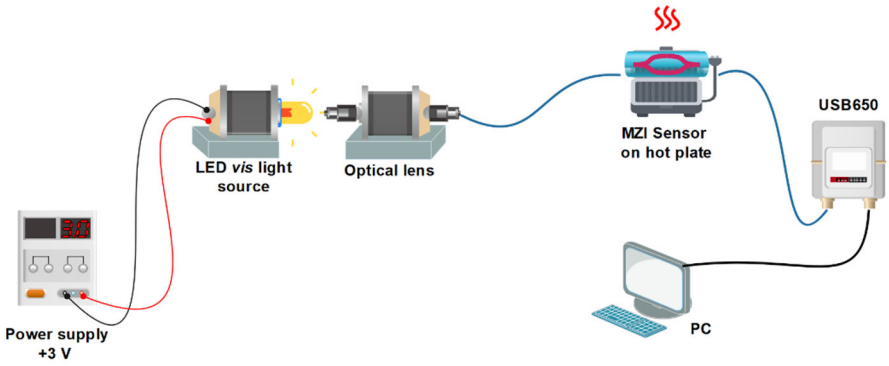

Figure 3. Experimental setup to measurement interference VIS pattern.

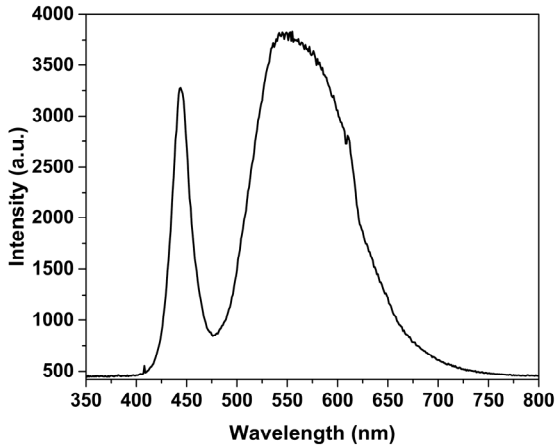

Figure 4. Spectral emission of LED Source.

The Table 1, shows a collection of samples of MZI´s with different parameters of waist diameter for T_1 and T_2 from 10 μm to 60 μm, the separation distance between two bi-taper is kept to $L = 3\ cm$ and waist length between 1.833 μm to 29.359 μm, are fabricated. In the home software, only the waist diameter is entered and another parameter is automatically calculated.

Table 1. Parameters of symmetric and asymmetric tapered MZI.

#MZI	**Taper 1 (T_1)**			**Taper 2 (T_2)**		
Waist diameter relation [μm] #[T_1-T_2]	Waist length [μm] L_1	Waist diameter [μm] W_1	Length [mm] D_1	Waist length [mm] L_2	Waist diameter [μm] W_2	Length [mm] D_2
1 [10-20]	5.051	10	2.526	7.330	20	3.665
2 [45-45]	6.130	45	3.065	6.130	45	3.065
3 [10-10]	5.051	10	2.526	5.051	10	2.526
4 [50-60]	1.833	50	0.916	29.359	60	14.679
5 [15-10]	8.481	15	4.241	5.051	10	2.526

2.2. Design and Fabrication of Core-Offset MZI

Preprints.org (www.preprints.org) | NOT PEER-REVIEWED | Posted: 14 March 2024 doi:10.20944/preprints202403.0858.v1

The Figure 5(a), shows a U-type MZI and was fabricated using SMF-28 (Thorlabs) with a core and cladding of 8.2 μm and 125 μm, respectively, and the schematic diagram of the experimental setup is similar to Figure 3. For the manufacturing process of the U-type MZI, we used three segments of SMF, a section of fiber length L between two SMFs, joined by Fitel S178A fusion splicer. First, a 70 cm section is cut with the fiber cleaver and fixed with masking tape to a flat aluminum bar, leaving about 7 cm of optical fiber at one end of the bar, see Figure 5(b). It is carefully placed in the left holder of the fusion splicer and the flat aluminum bar is placed on top of the lab jack of vertical travel L490, at the same height as the holders on the fusion splicer. Second, another of the optical fiber segments is placed in the right holder and the two core fibers are aligned. After, the right holder is displaced in $[-x_1, 0.0]$ axis direction, the splice is made in manual mode and the SMF-1300 program setting splicing with one discharge. Thirdly, we remove the spliced fiber and we cleave the second section of the interferometer length L. We used a ceramic fiber scribe CSW12-5 when L is short and the fiber cleaver when L is more than 4 cm in length, taking care not to break it. The cleaved part of the interferometer with length L is placed in the left holder and is a fusion spliced with another segment of 70 cm of fiber, and is aligned in the $[+x_2, 0.0]$ axis direction, we used the same configuration to fusion splicer. In order to analyze the influence of the offset distance on the propagation of the core and cladding modes, it was necessary to fabricate and test several symmetrical and asymmetrical interferometers, with length of 2.5cm, 4 cm and 5 cm, see Table 2.

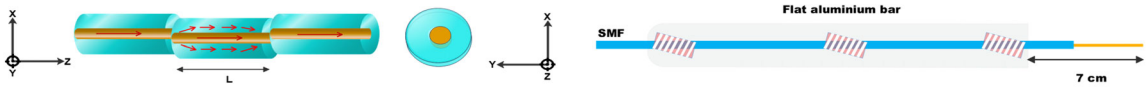

(**a**) (**b**)

Figure 5. Structure of MZI core-offset splicing technique. (**a**) U type MZI structure; (**b**) Fiber optics fixed on a flat aluminum bar.

The Table 2, shown a collection of samples of core offset MZI´s with different length segment of L=2.5 cm, 4 cm and 5 cm. For the analysis of spectrum emission, the MZIs were fabricated by displacement different in x, y axis.

Table 2. Parameters of symmetric and asymmetric SMF-SMF-SMF structure core offset MZI.

#MZI	Length L [cm]	First splice Displacement $[x_1, y_1]$ directions $[\mu m]$	Second splice Displacement $[x_2, y_2]$ directions $[\mu m]$
1	2.5	[-4.6, 0.0]	[+4.6,0.0]
2	4	[-3.0, 0.0]	[+3.0,0.0]
3	4	[-3.0, 0.0]	[+4.0,0.0]
4	4	[-4.0, 0.0]	[+4.0,0.0]
5	4	[-4.6, 0.0]	[+4.6,0.0]
6	4	[-5.0, 0.0]	[+4.0,0.0]
7	4	[-5.0, 0.0]	[+4.5,0.0]
8	4	[-6.0, 0.0]	[+5.0,0.0]
9	4	[-6.0, 0.0]	[+6.0,0.0]
10	5	[-4.6, 0.0]	[+4.6,0.0]

Preprints.org (www.preprints.org) | NOT PEER-REVIEWED | Posted: 14 March 2024 doi:10.20944/preprints202403.0858.v1

3. Results

The interference pattern was measured in tapered and core offset MZI´s. The results are presented in two parts:

3.1. Analysis to Tapered MZI

The Figure 6(a), shown the spectral emission and the Figure 6(b), the spatial frequency that are obtained by Fourier transform. In the Figure 6(a), the interference emission obtained for the MZI with a symmetrical waist length relation of ([45-45]) μm, is weak. For this case, we can see in the Figure 6(b), that the output of the interference pattern output is formed by the fundamental core mode and three cladding modes at $p{\sim}44\ nm$, $p{\sim}24\ nm$ and $p{\sim}17\ nm$, these spatial frecuencies are generated by the multimode fiber of the MZI [10-12] and there are more higher-order modes that contribute weakly to form the interference pattern with a not completely sinusoidal waveform. The best sinusoidal interference emission profile is obtained with an asymmetric waist length relation ([10-20]) μm and in the Figure 6(b), we can be see, that the interference is formed by the contribution of the fundamental core mode and a strong cladding mode in $p{\sim}24nm$. The period signal is rationed between spatial frequency and period sinusoidal components by $\nu = 1/p$ [17].

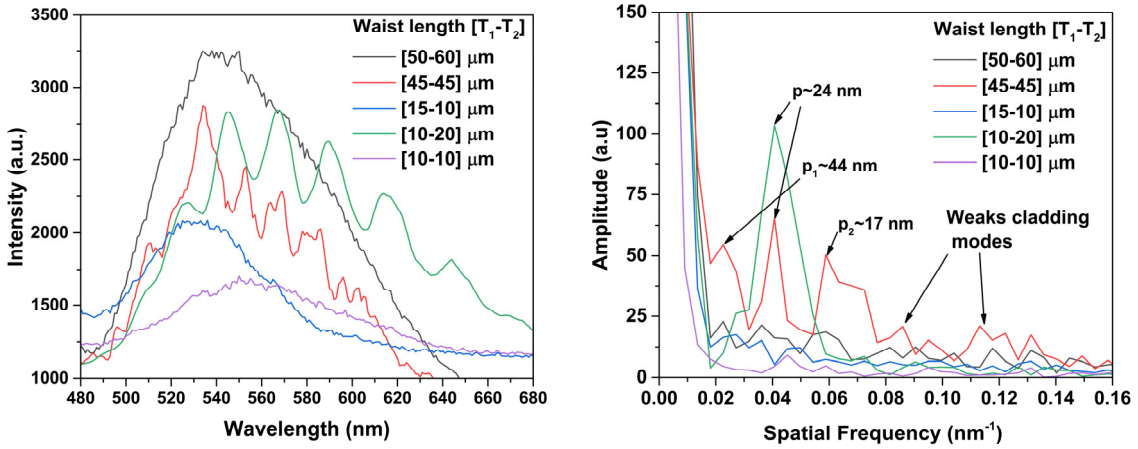

Figure 6. (**a**) Spectrum emission of #MZIs; (**b**) Spatial frequency spectrum by FTT.

The spatial frequency analysis is similar or almost adiabatic [5,16], because, the interference pattern of the asymmetric tapers of the fabricated is mainly formed by the fundamental core mode I_1 and cladding mode I_2. The asymmetric and symmetric MZI with a waist length relation of ([50-60], [15-10]) and ([10-10]) μm, see Figure 6(a); do not have an interference pattern due to their weak intensity of the cladding modes.

The spectral profile of the interferometer with waist length relation ([10-20]) μm are plotted in the Figure 7, the spectral response shape is a sinusoidal waveform, typical interference emission of a relation MZI [1]. The interference patterns are defined by optical path difference and its amplitude is in function of the fringe visibility or contrast, V and is defined based coherence theory by [1,22]:

$$V = \frac{I_{Max} - I_{Min}}{I_{Max} + I_{Max}} \tag{4}$$

 doi:10.20944/preprints202403.0858.v1

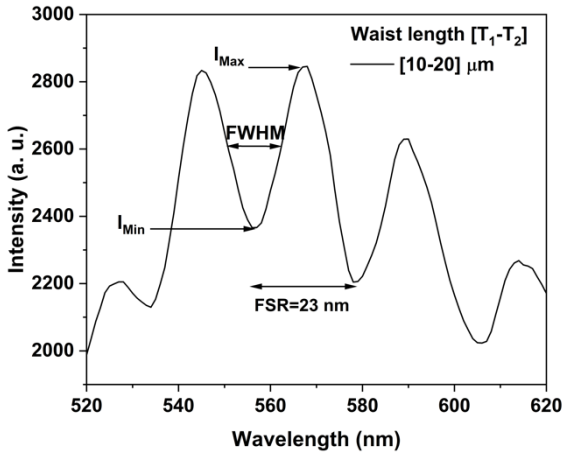

Figure 7. Transmission spectra of the taper MZI with waist length $[10-20]\ \mu m$.

Where I_{Max} is the maximal and I_{Min} is the minimal intensities of wave oscillations. The good fringes visibility V, can take a value between $0.1 \leq V \leq 1$. We find a visibility of V= 0.14, the FWHM= 13 nm and FSR= 23 nm, moreover, for other waist length relation MZI, the interference is weak or null. These parameters are very important for optical fiber sensor application [1,22].

3.2. Analysis to Core Offset MZI

The core-offset technique was studied experimentally with different displacement in the $[x, y]$ axis, in both the first and the second fusion splice, to fabricate the MZI were kept the length L at 4 cm. We fabricated from #2MZI to #9 MZI with different displacement in the x and y axis, as can see in the Table 2. The Figure 8(a) to 8(c) shows the evolution of interference spectrum dependent on the displacement of the $[x, y]$ axis in splicing fiber. We can see that the extinction ratio (ER) increases or decreases as the displacement [x,y] increases; i.e., for MZI #2, the displacement at the junction is ([-3.0,0.0] μm and [-3.0,0.0]) μm; for T1 and T2. For MZI #9, the displacement at the junction (([-6.0,0.0] μm and [+6.0,0.0]) μm, for T2.

The spatial frequency of the MZIs above mentioned is plotted in Figure 8(d), for the #5 MZI a strong cladding mode is present in $p \approx 15\ nm$ and is important in contributing to emission pattern interference; therefore, the interference pattern is due to the fundamental core and cladding mode in $p \approx 15\ nm$. For the #6 and #7 MZIs, the amplitude of the spatial frequency in $p \approx 15\ nm$ is smaller by 75% proximally that for the #5 MZI, but the output pattern also has a sinusoidal form, as can see in the Figure 8(b). We can see that, the interference patterns for another core-offset MZIs, are not completely sinusoidal waveform, due that it is formed by fundamental core mode and a number of high-order cladding modes. This is generated, when the white light is launched into the an SMF, higher-order modes (LP_{0m}) are excited [10,11]. We find, that the optimal displacement in the $[x, y]$ axis for the MZI is [-4.6,0.0] μm and [+4.6,0.0] μm, for the first and second junction splice, respectively.

 doi:10.20944/preprints202403.0858.v1

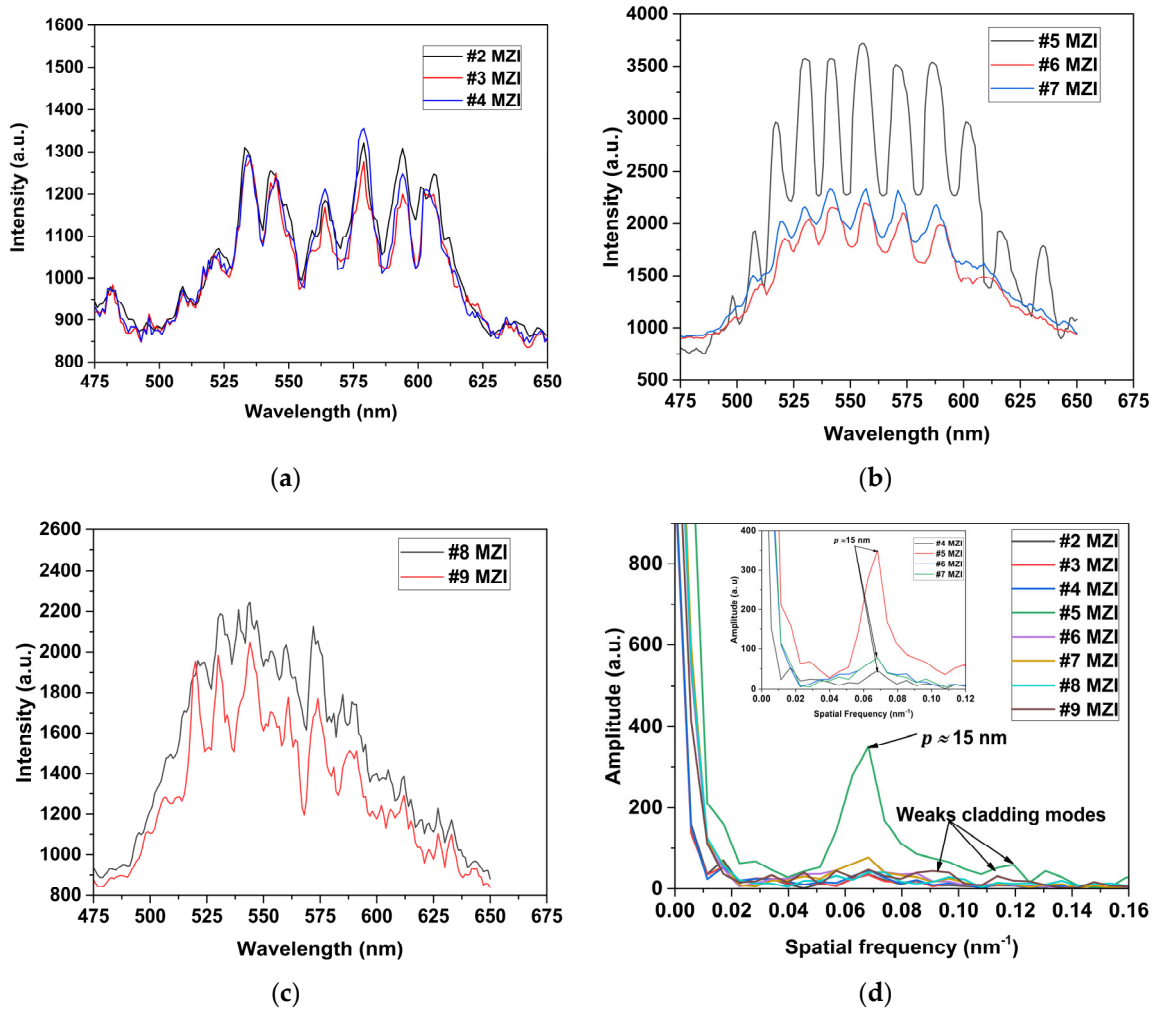

Figure 8. Spectrum emission of the core-offset MZI: (**a**) #2 MZI- #4 MZI, (**b**) #5 MZI- #7 MZI, (**c**) #8 MZI and #9 MZI, (**d**) Spatial frequency spectrum by FFT of the #2 MZI- #9 MZI, with a length of 4 cm.

The Figure 9, shown the spectra emission output of the #1, #5 and #10 MZIs with a displacement in the [x, y] axis, of [-4.6,0.0] μm and of [+4.6,0.0] μm, at first and the second fusion splice junction, respectively. We can see the output interference emission of the #1 MZI, Figure 9(a), with a visibility of V= 0.3, the FWHM= 13 nm and an FSR= 23 nm, for the #5 MZI, we obtained a V= 0.27, the FWHM= 8 nm, with an FSR= 17 (see Figure 9(b)) and for the #10 MZI, we obtained a V= 0.34, the FWHM= 3 nm with an FSR= 8 nm, see Figure 9(c). The Figure 9(d), shown the spatial frequency of MZIs with a length of L= 2.5 cm, L=4 cm and L=5 cm. The peak dominant intensity at zero is the core mode and the dominant core cladding modes are localized in $p \approx 21\ nm$, $p \approx 15\ nm$ and $p \approx 12\ nm$, respectively. It can also be seen that there are weak peaks that correspond to higher-order cladding modes, but their contribution is null to the interference pattern emission. Therefore, we can say that the interference emission is generated by core and cladding modes with different spatial frequencies because the length L is not the same at each interferometer.

 doi:10.20944/preprints202403.0858.v1

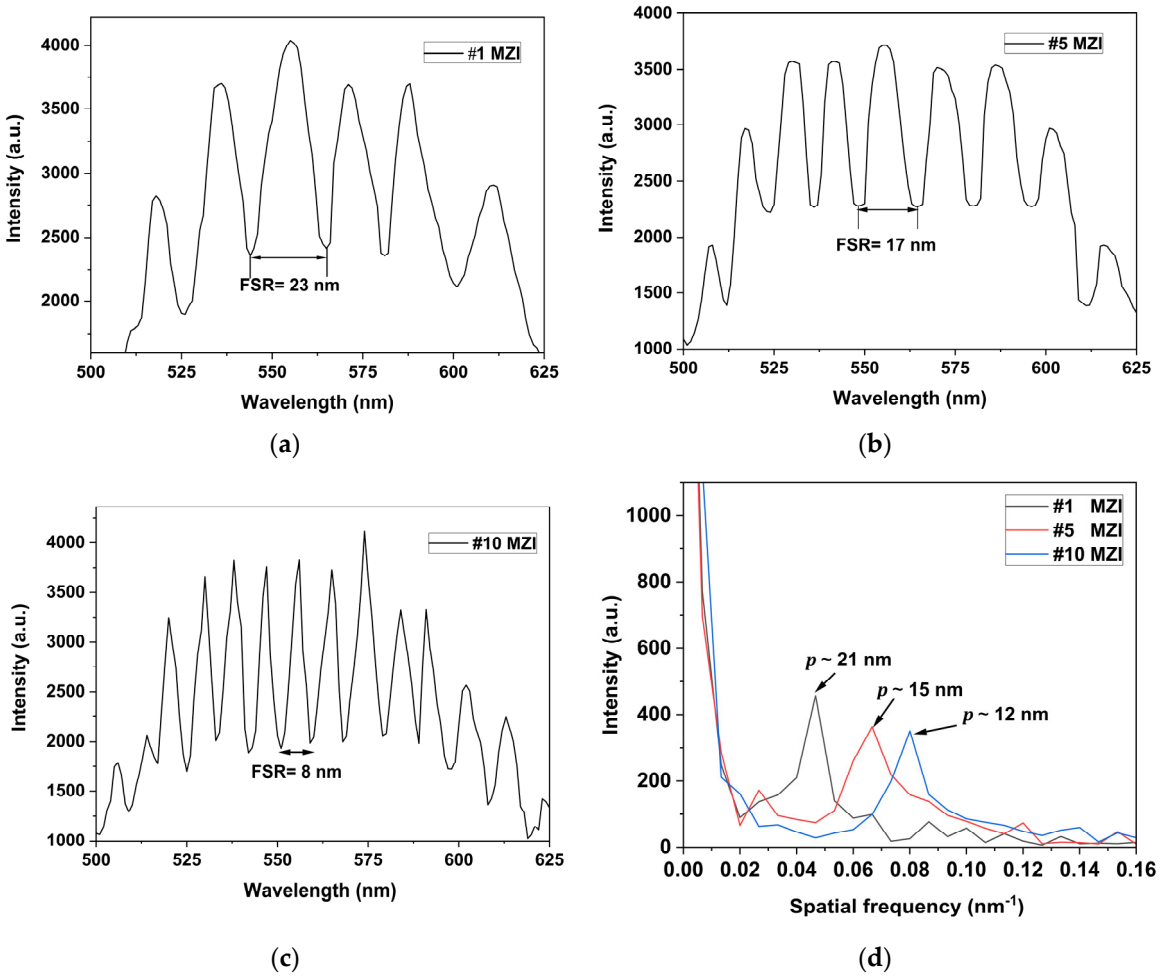

Figure 9. Shown the pattern interference emission: (**a**) The #1 MZI with L= 2.5 cm, (**b**) The #5 MZI with L= 4 cm, (**c**) The #10 MZI with L =5cm (**d**) Shown the spatial frequency of the #1, #5 and # 10 MZIs.

4. Discussion

Table 3 shows the comparison of the reported of fiber interferometer structure in infrared and visible regions and the range core-offset displacement is 5 μm to 40 μm with SMF-MZI MZI [2,3] and taper MZI structure [6,17], in the infrared region and for microcavity MZI structure in the visible region. In [3], is reported how a large lateral core-offset displacement effects the relative direction of the joints of two segments of SMF in the interference performance of an interferometer, and is obtained a visibility of V= 0.2 with a displacement of 6 μm and 40 μm. We can see that for our MZIs based core-offset, the best interference pattern is obtained at 4.6 μm, and in other displacements, the visibility of the fringes decreases considerably, up to 50%, V= 0.12 for #4 MZI, V=0.1 for #6 MZI and V= 0.08 for #7 MZI or is almost zero, Figure 8(a) and (b). Therefore, it is important to measure the displacement in the joints of two segments of fiber to fabricate an interferometer based on SMF-28 in the visible region, because a minimal increase in the displacement we can lose the interference emission. In was reported optical fiber sensor with symmetric and asymmetric taper MZI structures, visibility up of V=0.2. In [19], a visibility of V=0.5, was reported in an optical fiber SM-800 and SM-600, and in [21] a V=0.08 with MNF. Our proposed taper MZI with an asymmetric relation waist length ([10-20]) μm, has a sinusoidal profile of interference emission with a V=0.14 and an FSR=23 nm. These parameters are within the visibility range of $0.1 \leq V \leq 1$, [1,22]. Here, we used a SMF-28 with an LED source, and the visibility obtained are V=0.14 for taper MZI and V=0.3 for core-offset MZI

 doi:10.20944/preprints202403.0858.v1

Table 3. Comparison of the reported of fiber interferometer structure in infrared and visible region.

Interferometer structure and operation region	Core-offset [μm]	Interferometer length (cm)	FSR (nm)	Visibility	Ref.
Infrared region					
Core-offset MZI (SMF)	5	4	12	0.1	[2]
Core-Offset MZI (SMF)	6 to 40	3	15	0.2	[3]
Core-offset (SMF-Al coated)	30	2	16	0.7	[4]
Taper MZI (SMF)	-	2	19	0.2	[6]
Taper MZI (EDF)	-	4.5	12	0.25	[13]
Visible region					
Microcavity MZI (SMF-800)	-	-	50	0.5	[15]
Microcavity (MNF-SMF)	-	-	8	0.09	[17]
Core-offset (SMF)	4.6	2.5	23	0.3	This work

4.1. Sensing Application

Some setup based on the MZI have been proposed to temperature measurement [4], [18], which are useful as in the industry and medical applications. Therefore, with our core-offset MZI with length of 2.5 cm, were implement the experimental setup of the Figure 3. The sensor was fixed on a hot plate (Thermo Scientific Cimarec, Mod. SP131015) and the temperature response was measured by temperature detector Bosch GIS 500 (with a temperature range of $-30°C$ to $+500^oC$ and a resolution of $\pm 1.8\ ^o\ C$). The Figure 10(a), shown the temperature response that was detected in the range of 50^oC to 300^oC. We can see a variation of the intensity amplitude interference when the temperature increased. Because, as the temperature increases, the effective refractive index of both the cladding and core modes increases [4]. The peaks and dips A, C, E and B, D, respectively; were chosen to analyze the sensor sensitivity. The intensity amplitude variation versus temperature increased is shown in the Figure 10(b), present a good response to the change temperature. Sensitivities of 1.13 a.u./°C, 1.58 a.u./°C, 1.77 a.u./°C, 3.53 a.u./°C and 2.53 a.u./°C; with R^2 of 0.83077, 0.9538, 0.99393, 0.99769 and 0.97666, respectively, are achieved. The linear response is better to C, D and the best sensitivity and R^2, is the dip D.

 doi:10.20944/preprints202403.0858.v1

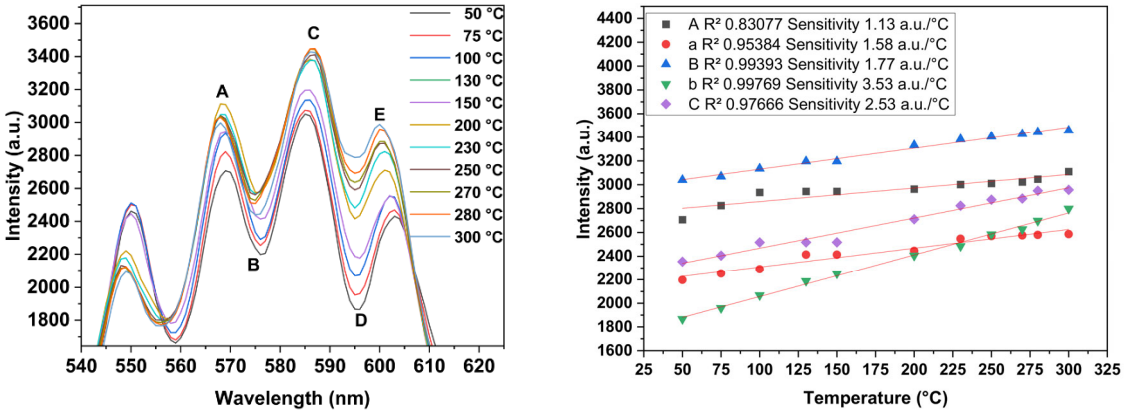

(**a**) (**b**)

Figure 10. (**a**) Spectrum emission of #MZIs. (**b**) Spatial frequency spectrum by FTT.

In the Figure 10, we can see that interference pattern was shifted a longer wavelength direction when the temperature increased. This is due, because the interference dips or resonant wavelength, expressed as [10-12]:

$$\lambda_{dip} = \frac{2\Delta 2\Delta n_{eff}}{2m+1} = \frac{2(\Delta n_{eff}^{m} + \beta\Delta T)(L_0 + \alpha\Delta T)}{2m+1} \quad (5)$$

where β is the thermos-optic coefficient difference core and cladding, and α is the thermal expansion coefficient. The resonant wavelength depends on the temperature by $2L_0\beta/(2m+1)$. Therefore, the interference patterns redshift as the temperature increase. The results of the analysis, are not significant, because the redshift of the peaks and dips is not lineal with increasing temperature.

The importance of the parameter of visibility range and the FSR in the interference emission is that to determinate its sensibility in the interferometers for the sensing application. By coating a layer of metal on the sensor, such as gold [23], platinum [24], aluminum [4] or another a thin metal to increase their sensitivity, these infrared reported. We think, that this type of sensor can have many applications with using a white light source.

5. Conclusions

Here, we have experimentally demonstrated the visible light interference in the taper and core-offset MZIs structure, using a standard SMF-28 for its fabrication. The obtained visibility fringes of V=0.14 and with an FSR= 23 nm for the taper MZI structure and with V=0.3, V=0.27 and V=0.34 with an FSR= 23 nm, 17 nm and 8nm, using a MZI with a length of L=2 cm, L= 4 cm and L= 5 cm, respectively. The core-offset MZI of 2.5 cm, was characterized by temperature sensor and the best sensitivity of 3.53 a.u./°C with a R^2 of 0.99769, is obtained. On the other hand, we believe that these structures can be used in the detection of other physical variables, as in refractive index, strain, pressure, chemical and biosensors.

Funding: This research received no external funding.

Acknowledgments: The Consejo Nacional de Humanidades, Ciencia y Tecnologias (CONAHCYT) is acknowledged for the support with the necessary resources to develop this project (number 745469).

Conflicts of Interest: The authors declare no conflicts of interest.

References

1. P. Hariharan, *Basics of Interferometry*. Elsevier, 2010.
2. L. Mao, P. Lu, Z. Lao, D. Liu, y J. Zhang, «Highly sensitive curvature sensor based on single-mode fiber using core-offset splicing», *Optics & Laser Technology*, vol. 57, pp. 39-43, abr. 2014, doi: 10.1016/j.optlastec.2013.09.036.

3. F. Yu, P. Xue, y J. Zheng, «Study of a large lateral core-offset in-line fiber modal interferometer for refractive index sensing», *Optical Fiber Technology*, vol. 47, pp. 107-112, ene. 2019, doi: 10.1016/j.yofte.2018.11.026.
4. E. I. Pacheco-Chacon *et al.*, «An aluminum-coated asymmetric core-offset Mach-Zehnder interferometer temperature sensor», *Optical Fiber Technology*, vol. 65, p. 102591, sep. 2021, doi: 10.1016/j.yofte.2021.102591.
5. D. Jauregui-Vazquez, J. W. Haus, A. B. H. Negari, J. M. Sierra-Hernandez, y K. Hansen, «Bitapered fiber sensor: Signal analysis», *Sensors and Actuators B: Chemical*, vol. 218, pp. 105-110, oct. 2015, doi: 10.1016/j.snb.2015.04.109.
6. T. K. Yadav, R. Narayanaswamy, M. H. Abu Bakar, Y. M. Kamil, y M. A. Mahdi, «Single mode tapered fiber-optic interferometer based refractive index sensor and its application to protein sensing», *Opt. Express*, vol. 22, n.º 19, p. 22802, sep. 2014, doi: 10.1364/OE.22.022802.
7. F. Yu, P. Xue, X. Zhao, y J. Zheng, «Investigation of an in-line fiber Mach–Zehnder interferometer based on peanut-shape structure for refractive index sensing», *Optics Communications*, vol. 435, pp. 173-177, mar. 2019, doi: 10.1016/j.optcom.2018.11.048.
8. X. Wang, C. Zhang, T. Huang, y X. Shu, «Multimode interferometer based on a core-offset singlemode-multimode-singlemode fiber structure», en *OSA Advanced Photonics Congress (AP) 2020 (IPR, NP, NOMA, Networks, PVLED, PSC, SPPCom, SOF)*, Washington, DC: Optica Publishing Group, 2020, p. JTu3F.11. doi: 10.1364/PSC.2020.JTu3F.11.
9. M. Shao, X. Qiao, H. Fu, H. Li, J. Zhao, y Y. Li, «A Mach–Zehnder interferometric humidity sensor based on waist-enlarged tapers», *Optics and Lasers in Engineering*, vol. 52, pp. 86-90, ene. 2014, doi: 10.1016/j.optlaseng.2013.07.023.
10. K. Tian, M. Zhang, G. Farrell, R. Wang, E. Lewis, y P. Wang, «Highly sensitive strain sensor based on composite interference established within S-tapered multimode fiber structure», *Opt. Express*, vol. 26, n.º 26, p. 33982, dic. 2018, doi: 10.1364/OE.26.033982.
11. X. Yang *et al.*, «Highly sensitive curvature sensor based on a sandwich multimode fiber Mach–Zehnder interferometer», *Opt. Express*, vol. 30, n.º 22, p. 40251, oct. 2022, doi: 10.1364/OE.469330.
12. X. Dong, H. Du, Z. Luo, K. Yin, y J. Duan, «Highly sensitive refractive index sensor based on novel Mach–Zehnder interferometer with multimode fiber–thin core fiber–multimode fiber structure», *Jpn. J. Appl. Phys.*, vol. 57, n.º 9, p. 092501, sep. 2018, doi: 10.7567/JJAP.57.092501.
13. H. Sun *et al.*, «Temperature and refractive index sensing characteristics of an MZI-based multimode fiber–dispersion compensation fiber–multimode fiber structure», *Optical Fiber Technology*, vol. 18, n.º 6, pp. 425-429, dic. 2012, doi: 10.1016/j.yofte.2012.05.003.
14. J. Zheng *et al.*, «Temperature and index insensitive strain sensor based on a photonic crystal fiber in line Mach–Zehnder interferometer», *Optics Communications*, vol. 297, pp. 7-11, jun. 2013, doi: 10.1016/j.optcom.2013.01.063.
15. R. Yang, L. Zhu, J. Li, T. Xu, y G. Sun, «High fringe visibility Mach-Zehnder interferometric sensor based on a Four-Core fiber», *Instrumentation Science & Technology*, vol. 48, n.º 3, pp. 326-337, may 2020, doi: 10.1080/10739149.2020.1719413.
16. K. Nazeri *et al.*, «Hollow-Core Photonic Crystal Fiber Mach–Zehnder Interferometer for Gas Sensing», *Sensors*, vol. 20, n.º 10, p. 2807, may 2020, doi: 10.3390/s20102807.
17. J. Gutiérrez Gutiérrez *et al.*, «A curvature sensing setup based on an asymmetric concatenated tapered Mach-Zehnder interferometer», *Optics & Laser Technology*, vol. 132, p. 106490, dic. 2020, doi: 10.1016/j.optlastec.2020.106490.
18. W. Lin *et al.*, «In-Fiber Mach–Zehnder Interferometer Sensor Based on Er Doped Fiber Peanut Structure in Fiber Ring Laser», *J. Lightwave Technol., JLT*, vol. 39, n.º 10, pp. 3350-3357, may 2021.
19. T. A. Eftimov, M. Janik, y W. J. Bock, «Microcavity In-Line Mach–Zehnder Interferometers Fabricated in Single-Mode Fibers and Fiber Tapers for Visible (VIS) and Near-Infrared (NIR) Operation», *J. Lightwave Technol.*, vol. 37, n.º 13, pp. 3351-3356, jul. 2019, doi: 10.1109/JLT.2019.2915784.
20. T. Eftimov, A. Arapova, M. Janik, y W. J. Bock, «Broad range bimodal microcavity in-line Mach-Zehnder interferometers», *Optics & Laser Technology*, vol. 145, p. 107503, ene. 2022, doi: 10.1016/j.optlastec.2021.107503.
21. Y. Li y L. Tong, «Mach-Zehnder interferometers assembled with optical microfibers or nanofibers», *Opt. Lett.*, vol. 33, n.º 4, p. 303, feb. 2008, doi: 10.1364/OL.33.000303.
22. J. Trinidad Guillen Bonilla, A. Guillen Bonilla, A. Casillas Zamora, H. Guillen Bonilla, V. María Rodríguez Betancourtt, y L. Gildo Ortiz, «The fringe visibility measurements on the complex s-plane: A novel method for the fringe visibility measurement», *Results in Physics*, vol. 38, p. 105586, jul. 2022, doi: 10.1016/j.rinp.2022.105586.
23. Y. Wang, Q. Huang, W. Zhu, M. Yang, y E. Lewis, «Novel optical fiber SPR temperature sensor based on MMF-PCF-MMF structure and gold-PDMS film», *Opt. Express*, vol. 26, n.º 2, p. 1910, ene. 2018, doi: 10.1364/OE.26.001910.

 doi:10.20944/preprints202403.0858.v1

24. X. Dong, Z. Xie, C. Zhou, K. Yin, Z. Luo, y J. Duan, «Temperature sensitivity enhancement of platinum-nanoparticle-coated long period fiber gratings fabricated by femtosecond laser», *Appl. Opt.*, vol. 56, n.º 23, p. 6549, ago. 2017, doi: 10.1364/AO.56.006549.